JPE 16-3-18

http://dx.doi.org/10.6113/JPE.2016.16.3.1004
ISSN(Print): 1598-2092 / ISSN(Online): 2093-4718

Model Parameter Correction Algorithm for Predictive Current Control of SMPMSM

Yonggui Li*, Shuang Wang†, Hua Ji*, Jian Shi*, and Surong Huang*

*,†School of Mechatronic Engineering and Automation, Shanghai University, Shanghai, China

Abstract

The inaccurate model parameters in the predictive current control of surface-mounted permanent magnet synchronous motor (SMPMSM) affect the current dynamic response and steady-state error. This paper presents a model parameter correction algorithm based on the relationship between the errors of model parameters and the static errors of *dq*-axis current. In this correction algorithm, the errors of inductance and flux are corrected in two steps. Resistance is ignored. First, the proportional relations between inductance and *d*-axis static current errors are utilized to correct the error of model inductance. Second, the flux is corrected by utilizing the proportional relations between flux and *q*-axis static current errors under the condition that inductance is corrected. An experimental study with a 100 W SMPMSM is performed to validate the proposed algorithm.

Key words: Model parameter, Parameter correction algorithm, Predictive current control, Surface-mounted permanent magnet synchronous motor

I. INTRODUCTION

Permanent magnet synchronous motors (PMSMs) are widely utilized in servo systems because of their high efficiency, high power density, and high torque current ratio [1], [2]. A high-performance PMSM servo system requires a fast-response current inner loop to ensure the high performance of speed and position loops. The traditional control methods of current loop include current hysteresis control and proportional-integral (PI) control [3], [4]. Current hysteresis control has the problems of variable switching frequency and large steady ripple. PI control is usually accompanied by overshoot because it requires tradeoffs between dynamic and steady-state performances. Both of them hardly meet the high-performance control requirements. With the development of high-speed digital signal processing technology, predictive current control, which requires complex computation, has been the focus of investigation in the high dynamic control of PMSM [5]-[7].

By using a motor model, predictive current control can predict the future current behavior to select a proper voltage vector, under which the current can follow the reference current in an optimal trajectory [8]-[12]. Predictive current controls can be divided into (at least) three classes, namely, direct predictive control (DPC), two-configuration predictive control (2PC), and pulse-width modulation (PWM) predictive control (PPC) [13]. DPC selects a voltage vector that minimizes a cost function and directly applies it to the inverter. Large current and torque ripples exist in DPC because the selected voltage vector is applied to the inverter in the entire sampling interval. A one–zero voltage vector is introduced in 2PC to overcome this major drawback of DPC. An active voltage vector and a zero voltage vector are applied to the inverter in a sampling interval to reduce the current and torque ripples. PPC calculates the ideal voltage vector, which is modulated through space vector PWM, and then applies it to the inverter. Two active voltage vectors and a zero voltage vector are applied to the inverter in one sampling interval to eliminate the current and torque errors. The control block diagrams of PPC and conventional PI control have the same structure; thus, the PPC controller can replace the PI controller. Therefore, PPC is investigated in this study.

Inaccurate model parameters affect the current dynamic response and steady-state error in predictive current control [14]-[21]. Many scholars have conducted extensive research to solve the problem of inaccurate parameters. In [14], a constraint-relaxing deadbeat predictive control strategy was proposed, in which the current offset constraint and the output voltage prediction method were modified to enhance the

Manuscript received Oct. 20, 2015; accepted Jan. 18, 2016
Recommended for publication by Associate Editor Bon-Gwan Gu.
†Corresponding Author: wang-shuang@shu.edu.cn
Tel: +86-136-0186-0669, Shanghai University
*School of Mechatronic Engineering and Automation, Shanghai University, China

system stability under the condition of inductance mismatch. A weighting factor was introduced in [15] to improve the system robustness. In [16], two adjacent sampling interval prediction models were subtracted to eliminate constant items to achieve close-loop control, which can avoid the steady-state error and eliminate the influence of flux. In [2], the predictive control method was improved by paralleling with an integrator to control *q*-axis current to eliminate the static torque current error caused by the flux error. All these methods can improve the performance of predictive current control with inaccurate parameters but cannot eliminate the model parameter error. In [17], the static current error was eliminated by introducing error integration in *d*-axis current control, and the model flux was dynamically adjusted according to the *q*-axis current error. However, the authors did not consider the influence of the inductance error on dynamic current performance. The model reference adaptive system (MRAS) was used in [18] and [19] to identify the model parameters of the motor online to eliminate the influence of the parameter error. However, MRAS requires an additional adjustable model, which increased the complexity of the system. In [20] and [21], the function between inductance and flux with i_d and i_q was established and utilized for predictive current control to eliminate the problem of inaccurate parameters. However, inductance-current and flux-current nonlinear maps were required. The maps were measured through repeated experimental procedures or with the help of software, which was not easy to obtain.

In this study, a model parameter correction algorithm for predictive current control of surface-mounted PMSM (SMPMSM) is proposed. The algorithm uses the proportional relation between inductance and *d*-axis static errors to correct the inductance error. The proportional relation between flux and *q*-axis static errors is utilized to correct the flux error under the condition that inductance is corrected. Inductance and flux converge to an actual value through the correction algorithm proposed in this study, and the problems of inaccurate inductance and flux are solved.

II. Predictive Current Control Method for SMPMSM

The stator voltage and state-space equations of the SMPMSM in the *d*-*q* rotor reference frame are provided by Equs. (1) and (2), respectively.

$$\begin{cases} u_d = Ri_d + L\dfrac{di_d}{dt} - \omega_e L i_q \\ u_q = Ri_q + L\dfrac{di_q}{dt} + \omega_e L i_d + \omega_e \psi_f \end{cases}, \quad (1)$$

$$\begin{cases} \dfrac{di_d}{dt} = \dfrac{1}{L}u_d - \dfrac{1}{L}Ri_d + \omega_e i_q \\ \dfrac{di_q}{dt} = \dfrac{1}{L}u_q - \dfrac{1}{L}Ri_q - \omega_e i_d - \dfrac{1}{L}\omega_e \psi_f \end{cases}, \quad (2)$$

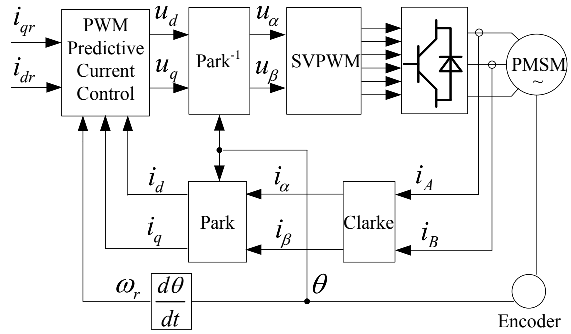

Fig. 1. Block diagram of PWM predictive current control.

where u_d, u_q and i_d, i_q are the *d*-*q* frame voltages and currents, respectively; L is stator inductance; R is stator resistance; Ψ_f is the flux established by the permanent magnet; ω_e is the electrical angular velocity of the rotor.

Control period T in a servo system is small. Consequently, ω_e is considered constant during each sampling period T. Based on the forward Euler approximation method, Equs. (1) and (2) can be discretized into Equs. (3) and (4), respectively.

$$\begin{cases} u_d[k] = Ri_d[k] + L\dfrac{i_d[k+1] - i_d[k]}{T} - \omega_e L i_q[k] \\ u_q[k] = Ri_q[k] + L\dfrac{i_q[k+1] - i_q[k]}{T} + \omega_e L i_d[k] + \omega_e \psi_f \end{cases} \quad (3)$$

$$\begin{cases} i_d[k+1] = \dfrac{T}{L}u_d[k] + \left(1 - \dfrac{T}{L}R\right)i_d[k] + T\omega_e i_q[k] \\ i_q[k+1] = \dfrac{T}{L}u_q[k] + \left(1 - \dfrac{T}{L}R\right)i_q[k] - T\omega_e i_d[k] - \dfrac{T}{L}\omega_e \psi_f \end{cases} \quad (4)$$

The PWM predictive current controller is built based on the voltage equation in Equ. (3). We suppose that i_{dr} and i_{qr} are the reference currents of *d*-axis and *q*-axis, respectively. The goal of predictive current control is for the actual currents to follow the reference currents after one modulation period. Therefore, we suppose that $i_d[k+1] = i_{dr}$ and $i_q[k+1] = i_{qr}$ and apply them to Equ. (3). Accordingly, we obtain the following equation.

$$\begin{cases} u_d[k] = Ri_d[k] + L\dfrac{i_{dr} - i_d[k]}{T} - \omega_e L i_q[k] \\ u_q[k] = Ri_q[k] + L\dfrac{i_{qr} - i_q[k]}{T} + \omega_e L i_d[k] + \omega_e \psi_f \end{cases} \quad (5)$$

The $u_d[k]$ and $u_q[k]$ calculated by Equ. (5) are the required voltage vectors that allow the current vectors to reach the reference currents after one modulation period.

Fig. 1 shows a block diagram of PWM predictive current control.

III. Parameter Sensitivity Analysis

Predictive current control is based on a motor model to calculate the desired voltage vectors. Inaccurate model parameters force the voltage vectors to deviate from the expected ones and thus result in poor control performance.

In this study, we suppose that the actual motor parameters

TABLE I
CURRENT RESPONSES OF DIFFERENT INDUCTANCE AND FLUX COMBINATIONS IN THEORY

Number	Inductance	Flux	Δi_d	Δi_q
1	L_0	Ψ_{f0}	=0	=0
2	$0.5L_0$	Ψ_{f0}	>0	=0
3	$1.5L_0$	Ψ_{f0}	<0	=0
4	L_0	$0.5\ \Psi_{f0}$	=0	<0
5	L_0	$1.5\ \Psi_{f0}$	=0	>0

are R_0, L_0, and Ψ_{f0}, and the predictive model parameters are R, L, and Ψ_f. During one control period, the voltage vectors calculated by Equ. (5) are applied to the actual motor, and the actual motor current response can be presented by Equ. (4). The following equations can be obtained by applying Equ. (5) to Equ. (4).

$$\begin{cases} i_d[k+1]=\dfrac{L}{L_0}i_{dr}+i_d[k]\left(\dfrac{T\Delta R-\Delta L}{L_0}\right)-T\omega_e i_q[k]\dfrac{\Delta L}{L_0} \\ i_q[k+1]=\dfrac{L}{L_0}i_{qr}+i_q[k]\left(\dfrac{T\Delta R-\Delta L}{L_0}\right)+T\omega_e i_d[k]\dfrac{\Delta L}{L_0}, \\ \quad +\dfrac{T}{L_0}\omega_e\Delta\psi_f \end{cases} \quad (6)$$

where $\Delta R = R - R_0$, $\Delta L = L - L_0$, and $\Delta\Psi_f = \Psi_f - \Psi_{f0}$ are the errors between model and actual motor parameters.

In a practical system, the order of magnitude of T is generally 10^{-4}, R is 10^{-1}, and L is from 10^{-3} to 10^{-2}. Considering that $T\Delta R$ is much smaller than ΔL, $T\Delta R$ is ignored, and Equ. (6) can be simplified as

$$\begin{cases} i_d[k+1]=\dfrac{L}{L_0}i_{dr}-\dfrac{\Delta L}{L_0}i_d[k]-\dfrac{\Delta L}{L_0}T\omega_e i_q[k] \\ i_q[k+1]=\dfrac{L}{L_0}i_{qr}-\dfrac{\Delta L}{L_0}i_q[k]+\dfrac{\Delta L}{L_0}T\omega_e i_d[k]+\dfrac{T}{L_0}\omega_e\Delta\psi_f \end{cases} .(7)$$

Considering that $i_d[k+1] = i_d[k]$ at steady-state operation, $i_d[k+1] = i_d[k]$ is applied to Equ. (7), and the static error of d-axis current response can be obtained.

$$\Delta i_d=-\frac{T}{L}\omega_e i_q[k]\Delta L, \quad (8)$$

where $\Delta i_d = i_d[k+1] - i_{dr}$.

Equ. (7) shows that $i_q[k+1]$ receives the dual effects of ΔL and $\Delta\Psi_f$. The current response of q-axis is analyzed under the condition of accurate inductance. Considering that $i_q[k+1] = i_q[k]$ at steady-state operation, ΔL=0 and $i_q[k+1] = i_q[k]$ are applied to Equ. (7). The static error of q-axis current response can also be obtained.

$$\Delta i_q=\frac{T}{L_0}\omega_e\Delta\psi_f, \quad (9)$$

where $\Delta i_q = i_q[k+1] - i_{qr}$.

Equ. (8) shows that Δi_d is proportional to ΔL and is not related to flux. Equ. (9) shows that Δi_q is proportional to $\Delta\Psi_f$ under the condition of accurate inductance. The current responses of different inductance and flux combinations are shown in Table I. A small inductance value causes the static current error of d-axis to be greater than zero. A large inductance value causes the static current error of d-axis to be less than zero. Under the condition of accurate inductance, a small flux value causes the static current error of q-axis to be less than zero. A large flux value causes the static current error of q-axis to be greater than zero.

IV. MODEL PARAMETER CORRECTION ALGORITHM

Based on the analysis in the preceding section, we propose a model parameter correction algorithm for predictive current control.

A. Inductance Correction Algorithm

Equ. (8) shows that the response error of d-axis static current error Δi_d is proportional to ΔL and is not related to flux. Δi_d and ΔL have an opposite sign ($\omega_e i_q > 0$ at steady-state operation). Equ. (10) is defined to correct the inductance error (if $\Delta i_d > 0$, then $\Delta L < 0$; the inductance should be increased and vice versa).

$$\begin{cases} 1): L[k]=L[k-1]+sign(\Delta i_d[k])C_L \\ 2): L[k]=L[k-1]+K_{IL}\Delta i_d[k] \\ 3): L[k]=L[k-1]+K_{PL}(\Delta i_d[k]-\Delta i_d[k-1])+K_{IL}\Delta i_d[k] \end{cases} ,(10)$$

where C_L is the inductance constant increment, K_{IL} is the inductance incremental integral coefficient, and K_{PL} is the inductance incremental proportionality coefficient.

In Equ. (10), Equ. (1) is the constant incremental mode, Equ. (2) is the integral incremental mode, and Equ. (3) is the proportional plus integral incremental mode. The first mode is relatively simple, but the second or the third mode is faster by selecting proper proportional and integral coefficients. The mode can be selected according to the control requirement of performance in a practical application.

If and only if $\Delta L = 0$, then $\Delta i_d = 0$. Equ. (10) converges with $\Delta L = 0$ and $\Delta i_d = 0$, which means that inductance L equals actual inductance L_0.

B. Flux Correction Algorithm

Equ. (9) shows that the response error of q-axis static current Δi_q is proportional to $\Delta\Psi_f$ under the condition of accurate inductance, and only one flux variable exists. The signs of Δi_q and $\Delta\Psi_f$ are identical (at steady-state operation). Equ. (11) is defined to correct the flux error (If $\Delta i_q > 0$, then $\Delta\Psi_f > 0$; the flux should be decreased and vice versa).

$$\begin{cases} 1): \psi_f[k]=\psi_f[k-1]-sign(\Delta i_q[k])C_\Psi \\ 2): \psi_f[k]=\psi_f[k-1]-K_{I\Psi}\Delta i_q[k] \\ 3): \psi_f[k]=\psi_f[k-1]-K_{P\Psi}(\Delta i_q[k]-\Delta i_q[k-1])-K_{I\Psi}\Delta i_q[k] \end{cases} ,(11)$$

where C_Ψ is the flux constant increment, $K_{I\Psi}$ is the flux

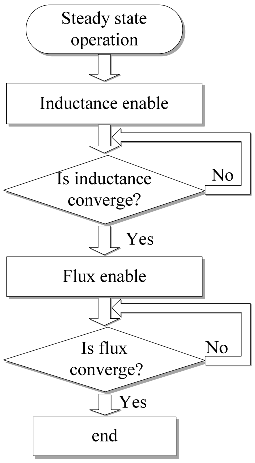

Fig. 2. Flow diagram of the model-parameter-setting algorithm.

incremental integral coefficient, and $K_{P\Psi}$ is the flux incremental proportionality coefficient.

In Equ. (11), Equ. (1) is the constant incremental mode, Equ. (2) is the integral incremental mode, and Equ. (3) is the proportional plus integral incremental mode. The mode can be selected according to the control requirement of performance in a practical application.

If and only if $\Delta\Psi_f = 0$, then $\Delta i_q = 0$. Equ. (11) converges with $\Delta\Psi_f = 0$ and $\Delta i_q = 0$, which means that flux Ψ_f equals actual flux $\Delta\Psi_{f0}$.

C. Flow of the Model Parameter Correction Algorithm

The preceding analysis indicates that the flux is corrected under the condition of accurate inductance. Hence, the flow of the model parameter correction algorithm must correct the inductance first and then the flux. The flow diagram of the model parameter correction algorithm is shown in Fig. 2. At steady-state operation (constant speed), the inductance correction algorithm is enabled first. Then, the flux correction algorithm is enabled after inductance convergence. The entire algorithm is completed when the flux converges.

The block diagram of the PWM predictive current control with the model parameter correction algorithm is shown in Fig. 3. A block called parameter correction algorithm is added in Fig. 3 unlike the diagram in Fig. 1. Reference and feedback currents are utilized to correct inductance and flux errors.

V. EXPERIMENTAL RESULTS AND ANALYSIS

An experimental platform is established to verify the correctness of the parameter sensitivity analysis for predictive current control and the proposed model parameter correction algorithm. This platform utilizes a Xilinx Spartan-6 field-programmable gate array (FPGA) as the main control chip and two identical SMPMSMs to build a drag system. The specifications of the SMPMSMs utilized in this research are listed in Table II.

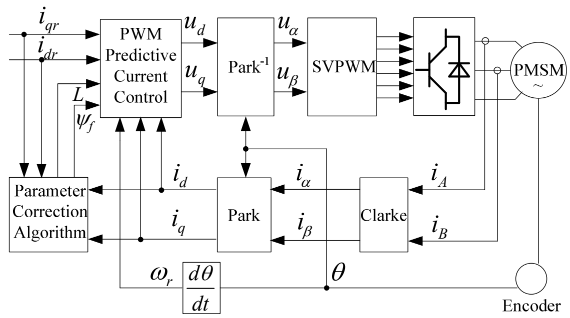

Fig. 3. Block diagram of the model parameter correction algorithm for PWM predictive current control.

TABLE II
MOTOR SPECIFICATION

Parameter	Value
Phase resistance of the stator	0.3 Ω
Inductance of the stator	0.001 H
Flux of permanent magnet	0.0086 Wb
Number of pole pairs	4
Rated current	4 A
Rated power	0.1 kW
Rated speed	3000 rpm

The sampling period of the current loop is set to 100 μs. The high-speed computing performance of FPGA makes the time delay only 7.4 μs from current sampling to PWM updating, accounting for 7.4% of the sampling period. Therefore, the instant duty cycle update strategy mentioned in [4] is used in this experiment.

The experimental data are sent to the upper computer through the communication module for monitoring and processing. A total of 1000 N (N channels within 0–100 ms) data are stored in the FGPA random-access memory and then read and sent to ensure that the data in each sampling period can be sent without loss.

A. Experiment on Parameter Sensitivity

Experiments are conducted for parameter sensitivity analysis. No speed loop exists in these experiments, and q-axis reference current i_{qr} is set from 0 A to 4 A at 10 ms moment and set from 4 A to 2 A at 20 ms moment. The waveforms during 8–25 ms and the amplified waveform near 10 and 20 ms are recorded. The experimental results of five different conditions (see Table I) are provided (Figs. 4–8).

Fig. 4 shows the experimental results when $L = L_0$ and $\Psi_f = \Psi_{f0}$. The current rise time from 0 A to 4 A is $3T$ (three control periods). u_q (per-unit value) reaches the limiting value in the first $2T$. The falling time from 4 A to 2 A is $1T$ only, during which u_q is not saturated. The static errors of d-axis and q-axis are zero. The predictive current control with accurate parameters thus has a good control performance.

Figs. 5 and 6 show the experimental results when $L = 0.5L_0$ and $\Psi_f = \Psi_{f0}$ and when $L = 1.5L_0$ and $\Psi_f = \Psi_{f0}$, respectively. Figs. 7 and 8 show the experimental results when $L = L_0$ and Ψ_f

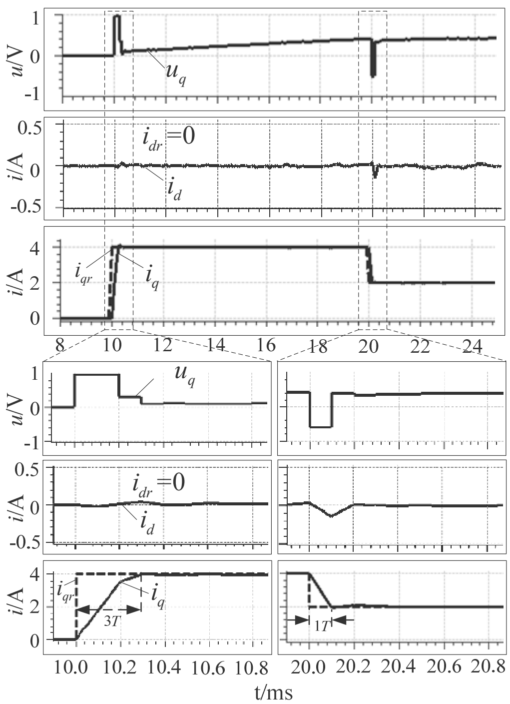

Fig. 4. Experimental result when L=L_0 and $\Psi_f = \Psi_{f0}$.

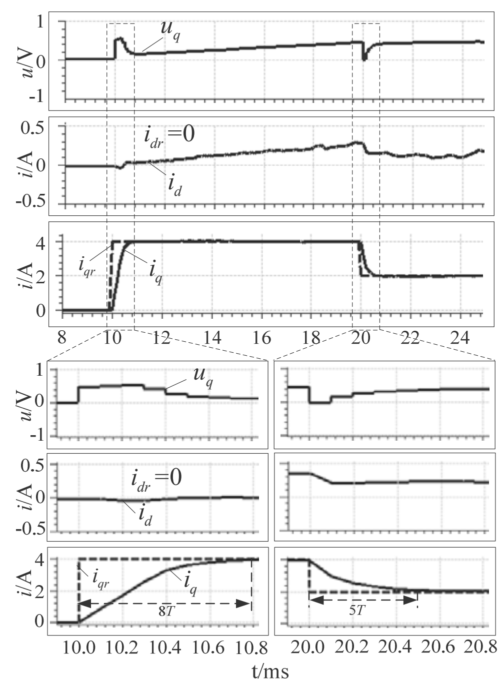

Fig. 5. Experiment result when L=0.5L_0 and $\Psi_f = \Psi_{f0}$.

= 0.5 Ψ_{f0} and when L = L_0 and Ψ_f = 1.5 Ψ_{f0}, respectively. The experimental results in Figs. 4–8 are concluded in Table III.

Table III verifies that the d-axis static current error is only related to the inductance error. The d-axis static current error is greater than zero with small model inductance (Fig. 5) and less than zero with large model inductance (Fig. 6). Under the condition of accurate inductance, the q-axis static current error is only related to the flux error. The error is greater than zero

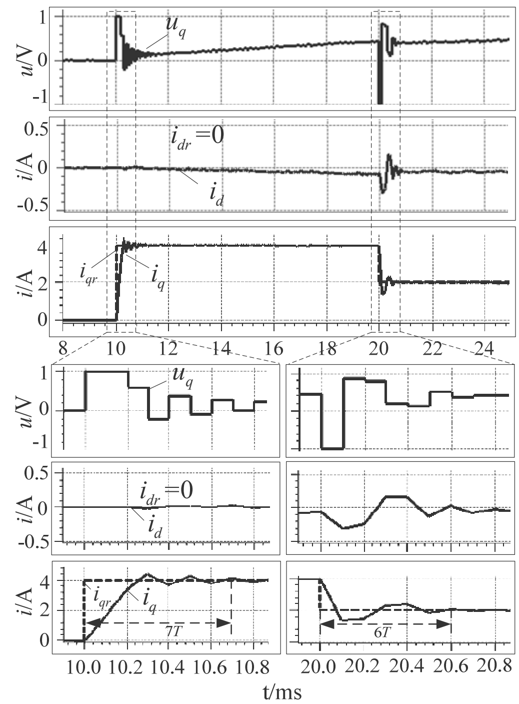

Fig. 6. Experimental result when L=1.5L_0 and $\Psi_f = \Psi_{f0}$.

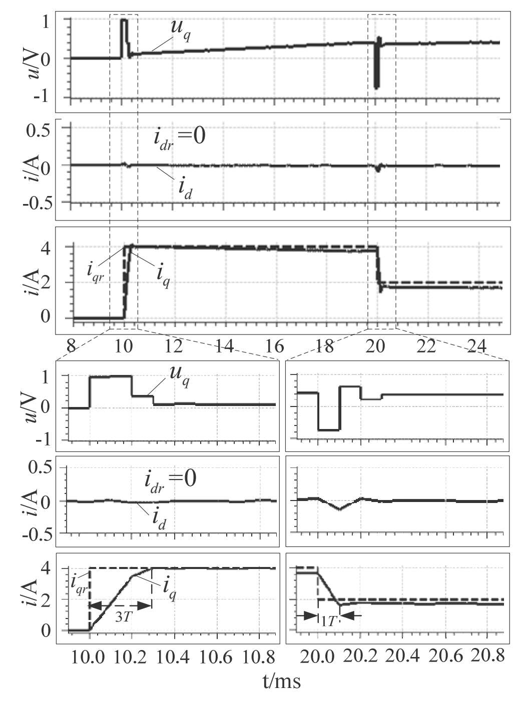

Fig. 7. Experimental result when L=L_0 and Ψ_f = 0.5 Ψ_{f0}.

with large model flux (Fig. 7) and less than zero with small model flux (Fig. 8). The experimental results (Table III) are consistent with the analysis results (Table I), and the correctness of the analysis is verified.

B. Experiment on the Model Parameter Correction Algorithm

The constant incremental mode for the inductance and flux

TABLE III
CURRENT RESPONSES OF DIFFERENT INDUCTANCE AND FLUX COMBINATIONS

Inductance	Flux	T_{0A-4A}	T_{4A-2A}	Δi_d	Δi_q
L_0	Ψ_{f0}	$3T$	$1T$	$= 0$	$= 0$
$0.5L_0$	Ψ_{f0}	$8T$	$5T$	> 0	$= 0$
$1.5L_0$	Ψ_{f0}	$7T$	$6T$	< 0	$= 0$
L_0	$0.5\,\Psi_{f0}$	$3T$	$1T$	$= 0$	< 0
L_0	$1.5\,\Psi_{f0}$	$3T$	$1T$	$= 0$	> 0

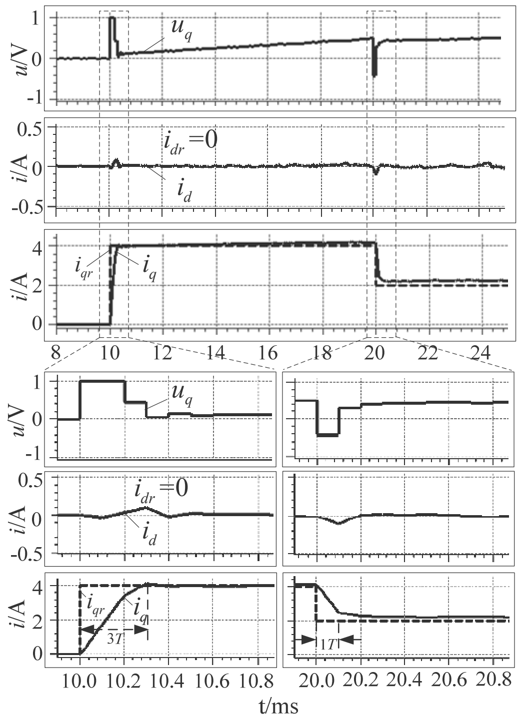

Fig. 8. Experimental result when L=L_0 and Ψ_f= 1.5 Ψ_{f0}.

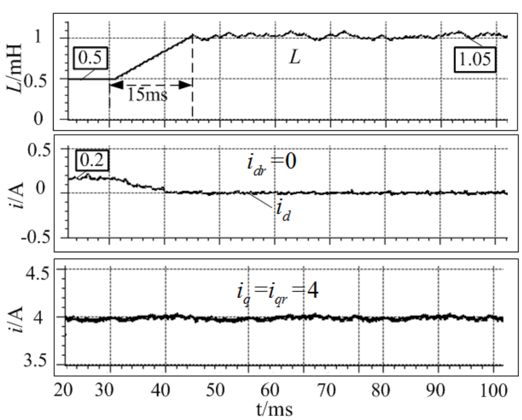

Fig. 9. Experimental result when L=0.5L_0 and Ψ_f= Ψ_{f0}.

correction algorithm is selected to simplify the system and save on FPGA logic resources. A steady-state operation with a reference speed of 1500 r/min and q-axis current of 4 A by loading is implemented for the experiment. The experimental results of the model parameter correction algorithm are provided (Figs. 9-12).

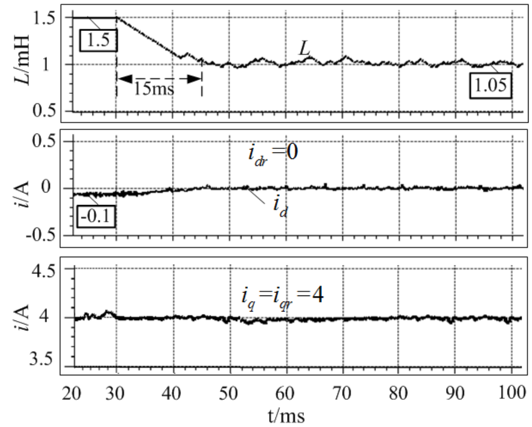

Fig. 10. Experimental result when L=1.5L_0 and Ψ_f= Ψ_{f0}.

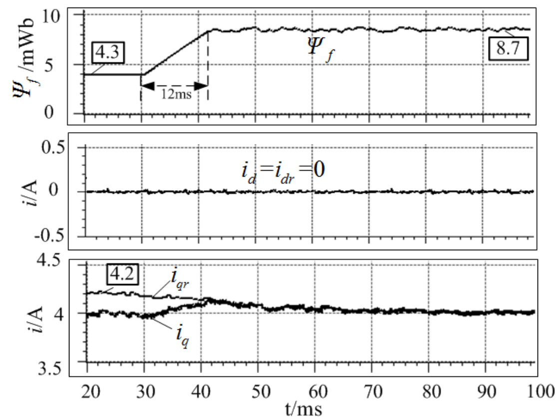

Fig. 11. Experimental result when L=L_0 and Ψ_f=0.5 Ψ_{f0}.

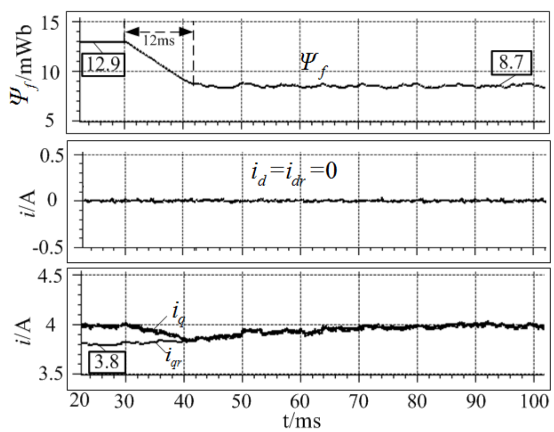

Fig. 12. Experimental result when L=L_0 and Ψ_f=1.5 Ψ_{f0}.

Inductance correction is not related to flux. Therefore, only the experimental results when L=0.5L_0 and Ψ_f= Ψ_{f0} and when L=1.5L_0 and Ψ_f= Ψ_{f0} are provided. Figs. 9 and 10 present the experimental results of the inductance correction algorithm when L = 0.5L_0 and L = 1.5L_0, respectively. The inductance converges to the actual value with a convergence time of approximately 15 ms and a convergence error of approximately 5%. The convergence error is not related to the initial value, and the inductance converges with L = L_0 and Δi_d = 0.

Figs. 11 and 12 show the experimental results of the flux correction algorithm when $\Psi_f = 0.5\Psi_{f0}$ and $\Psi_f = 1.5\Psi_{f0}$ after inductance convergence, respectively. The flux converges to the actual value with a convergence time of approximately 12 ms and a convergence error of approximately 1.2%. The convergence error is not related to the initial flux value, and the flux converges with $\Psi_f = \Psi_{f0}$ and $\Delta i_q = 0$.

The experimental results (Figs. 9–12) verify the correctness and feasibility of the proposed model parameter correction algorithm.

VI. Conclusion

Given its excellent control performance, predictive current control is attractive in the high-performance control of SMPMSM. Predictive current control is sensitive to the errors of model parameters. Based on the analysis of the relations between model parameter and current static errors, a model parameter correction algorithm was developed for predictive current control. Considering that the *d*-axis static current error is only related to the inductance error, the algorithm corrects the inductance and converges with $\Delta L = 0$ and $\Delta i_d = 0$. Under the condition that the inductance converges, the *q*-axis static current error is proportional to the flux error. By utilizing this proportional relation, the flux is corrected and converges with $\Delta\Psi_f = 0$ and $\Delta i_q = 0$. The experimental results show that inductance and flux converge to actual values with convergence times of approximately 15 and 12 ms and with convergence errors of approximately 5% and 1.2%, respectively. These results verify the correctness and feasibility of the proposed algorithm.

Acknowledgment

This work was supported by the Doctoral Program of Higher Education of China under Grant 20113108110008 and the National Natural Science Foundation of China under Grant 51507097.

References

[1] S. Wang, W. J. Zhu, J. Shi, H. Ji, and S. Huang, "A high performance permanent magnet synchronous motor servo system using predictive functional control and kalman filter," *Journal of Power Electronics*, Vol. 15, No. 6, pp. 1547-1558, Nov. 2015

[2] W. H. Wang and X. Xiao, "A current control for permanent magnet synchronous motors with high dynamic performance," in *Proc. the CSEE*, Vol. 33, No. 21, pp. 117-123, Jul. 2013.

[3] M. P. Kazmierkowski and L. Malesani, "Current control techniques for three-phase voltage-source PWM converters：a survey," *IEEE Trans. Ind. Electron.*, Vol. 45, No. 5, pp. 691-703, Oct. 1998.

[4] M. W. Naouar, E. Monmasson, and A. A. Naassani, "FPGA- based current controllers for AC machine drives – A review," *IEEE Trans. Ind. Electron.*, Vol. 54, No. 4, pp. 1907-1925, Aug. 2007.

[5] R. Kennel and A. Linder, "Predictive control of inverter supplied electrical drives," *Power Electronics Specialists Conference, PESC. 2000 IEEE 31st Annual*, pp. 761-766, 2000.

[6] H. Le-Huy, K. Slimani, and P. Viarouge, "Analysis and implementation of a real-time predictive current controller for permanent-magnet synchronous servo drives," *IEEE Trans. Ind. Electron.*, Vol. 41, No. 1, pp. 110-117, Feb. 1994.

[7] J. C. Moreno, J. M. E. Huerta, and R. G. Gil, "A robust predictive current control for three-phase grid-connected inverters," *IEEE Trans. Ind. Electron.*, Vol. 56, No. 6, pp. 1993-2004, Jun. 2009.

[8] P. Cortes, M. P. Kazmierkowski, and R. M. Kennel, "Predictive control in power electronics and drives," *IEEE Trans. Ind. Electron.*, Vol. 55, No. 12, pp. 4312-4324, Dec. 2008.

[9] G. Cimini, V. Fossi, and G. Ippoliti, "Model predictive control solution for permanent magnet synchronous motors," *39th Annual Conference on IEEE Industrial Electronics (IECON), Vienna, Austria*, pp. 5824-5829, 2013.

[10] H. T. Moon, H. S. Kim, and M. J. Youn, "A discrete-time predictive current control for PMSM," *IEEE Trans. Ind. Electron.*, Vol. 18, No. 1, pp. 464-472, Jan. 2003.

[11] J. Rodríguez, J. Pontt, and C. A. Silva, "Predictive current ontrol of a voltage source inverter," *IEEE Trans. Ind. Electron.*, Vol. 54, No.1, pp. 495-503, Feb. 2007.

[12] L. Y. Gao, D. Lu, and G. Z. Zhao, "Current control for PMSM based on model predictive control with automatic differentiation," *Electric Machines and Control*, Vol. 16, No. 10, pp. 38-43, Oct. 2012.

[13] F. Morel, X. Lin-Shi, and J. M. Retif, "A comparative study of predictive current control schemes for a permanent magnet synchronous machine drive," *IEEE Trans. Ind. Electron.*, Vol. 56, No. 7, pp. 2715-2728, Jul. 2009.

[14] H. J. Wang, D. G. Xu, and M. Yang, "Improved deadbeat predictive current control strategy of permanent magnet motor drives," *Industrial Electronics and Applications (ICIEA), 2011 6th IEEE Conference*, Vol. 49, pp. 1260-1264, 2011.

[15] L. Niu, M. Yang, and D. G. Xu, "Predictive current control for Permanent Magnet Synchronous Motor based on deadbeat control," *Industrial Electronics and Applications (ICIEA), 2012 7th IEEE Conference on. IEEE*, pp. 46-51, 2012.

[16] W. H. Wang and X. Xiao, "Current control method for PMSM with high dynamic performance," *Electric Machines & Drives Conference (IEMDC), 2013 IEEE International*, pp. 1249-1254, 2013.

[17] G. Wang, M. Yang, L. Niu, X. Gui, and D. Xu, "Improved predictive current control with static current error elimination for permanent magnet synchronous machine," *Industrial Electronics Society, IECON 2014 - 40th Annual Conference of the IEEE*, pp.661-667, 2014.

[18] W. H. Wang and X. Xiao, "Research on predictive control for PMSM based on online parameter identification," *IECON 2012-38th Annual Conference on IEEE Industrial Electronics Society*, *IEEE*, pp. 1982-1986, 2012.

[19] Q. Xu, Z. C. Jia, and L. R. Li, "Adaptive predictive current control of permanent magnet synchronous motor," *Electric*

Drive, No. 4, pp. 19-24, Jul. 1997.

[20] A. Imura, T. Takahashi, and M. Fujitsuna, "Improved PMSM model considering flux characteristics for model predictive-based current control," *Ieej Transactions on Electrical & Electronic Engineering*, Vol. 10, No. 1, pp. 192-100, Jan. 2015.

[21] G. Angelone, A. D. Pizzo, and I. Spina, "Model predictive control for PMSM with flux–current nonlinear maps," *International Symposium on Power Electronics, Electrical Drives, Automation & Motion*, pp. 848-853, 2014.

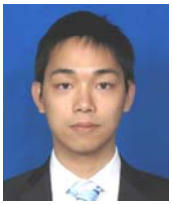

Yonggui Li was born in Guangxi, China, in 1991. He received his B.S. degree in automation from Shanghai University, Shanghai, China, in 2014. He is presently a postgraduate student at Shanghai University, Shanghai, China. His current research interests include new energy vehicles, intelligent control theory, power electronics, and high-performance servo control systems.

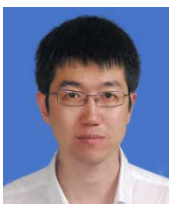

Shuang Wang was born in Jilin, China, in 1977. He received his B.S., M.S., and Ph.D. degrees in electrical engineering from Harbin Institute of Technology, Harbin, China, in 2000, 2005, and 2009, respectively. Since 2010, he has been with the School of Mechatronic Engineering and Automation, Shanghai University, Shanghai, China, where he is presently working as an assistant professor. His current research interests include intelligent control theory and its application to new energy vehicles, power electronics, and servo control systems.

Hua Ji was born in Qingdao, China, in 1977. She received her M.S. degree in electrical engineering from Nanjing University of Aeronautics and Astronautics, Nanjing, China, in 2004. Since 2004, she has been with the Department of Electrical and Electronic Engineering, Shandong University of Technology, Zibo, China, where she is presently an associate professor. Her current research interests include the study of high-performance servo control systems.

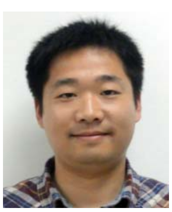

Jian Shi was born in Henan, China, in 1982. He received his M.S. degree in electrical engineering from Fuzhou University, Fuzhou, China, in 2007 and his Ph.D. degree in electrical engineering from Harbin Institute of Technology, Harbin, China, in 2013. From 2007 to 2010, he worked for ThyssenKrupp Elevator Co., China, as a research engineer. Since 2014, he has been a post-doctoral researcher at Shanghai University, Shanghai, China. His current research interests include electric machines, power electronics, and control systems.

Surong Huang was born in Shanghai, China. He received his diploma degree from Shanghai Institute of Mechanics, Shanghai, China, in 1977. In 1977, he joined Shanghai Institute of Mechanics, where he was promoted to associate professor and then professor in 1993 and 2001, respectively. He was a visiting faculty member at the Department of Electrical and Computer Engineering, University of Wisconsin, Madison, WI, USA, from 1995 to 1996 and from 1998 to 2000. He is currently a professor and doctoral supervisor at the Department of Automation, Shanghai University, Shanghai, China. He is engaged in the research and development of new types of electrical machines and drive systems. His current research interests include design, control, modeling, and simulation of electrical machines and AC drives and vibration and noise analyses of electrical machines. He has published more than 100 papers on these topics.